Applied Catalysis B: Environmental 246 (2019) 242–253

Contents lists available at ScienceDirect

Applied Catalysis B: Environmental

journal homepage: www.elsevier.com/locate/apcatb

# Investigation of the robust hydrothermal stability of Cu/LTA for $NH_3$-SCR reaction

Aiyong Wang[a], Prakhar Arora[a], Diana Bernin[a], Ashok Kumar[b], Krishna Kamasamudram[b], Louise Olsson[a,*]

[a] Competence Centre for Catalysis, Chemical Engineering, Chalmers University of Technology, Gothenburg, SE, 412 96, Sweden
[b] Cummins Inc., 1900 McKinley Avenue, MC 50183, Columbus, IN, 47201, USA

ARTICLE INFO

*Keywords:*
Cu/LTA
Standard SCR
Fast SCR
Hydrothermal aging
Cu species

ABSTRACT

Recently copper ion-exchanged LTA zeolites were proved to be robust for $NH_3$-SCR reaction. In this study, Cu/LTA catalysts with Si/Al = 15 and Cu/Al = 0.4 were synthesized via incipient wetness impregnation (IWI) method, following degreening/hydrothermal aging at different temperatures (750, 800, 850, 900 °C), and used to catalyze standard SCR, fast SCR and $NH_3$/NO oxidation reactions. Catalysts were characterized with surface area/pore volume, powder X-Ray diffraction (XRD), nuclear magnetic resonance (NMR), $H_2$-temperature programmed reduction ($H_2$-TPR) and in situ Diffuse Reflectance Infrared Fourier Transform Spectra (DRIFTS). Through the BET surface areas, XRD and NMR results, it can be found that the framework structure stability of Cu/LTA catalysts during hydrothermal aging was outstanding, even after harsh aging at 900 °C. Moreover, various Cu species, including Z-$Cu^{2+}$, Z-$[Cu(OH)]^+$ and $CuO_x$ clusters, were quantified for Cu/LTA catalysts hydrothermally aged under various temperatures with $H_2$-TPR and in situ DRIFTS. An imperative finding in this study is the exceptional hydrothermal stability of $[Cu(OH)]^+$ and the gradual conversions of both $Cu^{2+}$ and $CuO_x$ clusters to $[Cu(OH)]^+$ with increasing aging temperature. It is worth noting that this phenomenon is exactly the opposite of Cu/SSZ-13. As it is known from the literature (Song et al., 2017), the formation of $CuO_x$ not only decreases the selectivity of $NO_x$ conversion, but also can cause deterioration of zeolite structure, since the ion-exchanged copper stabilizes the zeolite. This may also explain why the hydrothermal stability of Cu/LTA samples is outstanding.

## 1. Introduction

Lean-burn engines, where combustion occur under the environment of excess oxygen (air-fuel ratio 14–22), emerged because of fuel-economy advantages over stoichiometric engines. In addition, these engines also results in reduced emission of gases such as CO and HCs in the exhaust. However, the removal of $NO_x$ is more difficult from lean exhaust compared to stoichiometric and the removal of $NO_x$ under excess oxygen conditions has therefore resulted in significant research in the field of catalysis [2–5]. Selective catalytic reduction (SCR) is commercially used for $NO_x$ abatement and has been subject of many studies for more than two decades. Among these studies, research on molecular sieve catalytic materials has been particularly active for the last 10 years [6–10]. Chabazite (CHA) framework zeolites, e.g., SSZ-13 and SAPO-34, are the most studied materials in recent years, however, pure SSZ-13 or SAPO-34 have very poor $NO_x$ abatement in the $NH_3$-SCR reaction. Researchers have successively modified CHA zeolites with transition metals such as Cu and Fe, which greatly improved the catalytic activity for $NH_3$-SCR [11–13]. At present, studies on modified CHA catalysts have been gaining momentum, especially Cu ion-exchanged catalysts, such as Cu/SSZ-13. Catalyst systems based on these materials have already been applied in diesel engines in US and Europe-based vehicles [14,15].

However, Cu/SSZ-13 deactivates when exposed to high temperature, for example hydrothermal aging at 850 °C inevitably leads to a substantial loss in surface area and pore volume, as well as significant activity loss [1,16,17]. Therefore, with more stringent environmental requirements in most countries, a more robust zeolite would be very beneficial for the next generation of $NO_x$ abatement catalyst.

Zeolite LTA (Linde Type A) was first successfully synthesized by Breck et al. in 1956 [18], since then it has been widely used as adsorbent, ion-exchanger and gas separation filter in industry [19–21]. However, its capability in catalytic applications was limited owing to its poor hydrothermal stability, which is eventually a consequence of the

* Corresponding author.
*E-mail address:* louise.olsson@chalmers.se (L. Olsson).

https://doi.org/10.1016/j.apcatb.2019.01.039
Received 11 November 2018; Received in revised form 9 January 2019; Accepted 16 January 2019
Available online 17 January 2019

low framework Si/Al ratio (up to three). Year 2004, Corma et al. [22], using a supramolecular organic structure-directing agent through π-π type interactions, synthesized LTA structure zeolite exhibiting Si/Al ratio up to infinity with exceptional hydrothermal stability. Recently, Boal et al. [23] and Jo et al. [24] reported a simple synthesized Organic Structure-Directing Agent (OSDA), 1,2-dimethyl-3-(4-methylbenzyl) imidazolium (12DM3(4MB)I), for the preparation of LTA zeolite with a wide Si/Al ratio from 8.3 to ∞, under relatively simple synthesizing conditions. Moreover, the latter group found that Cu/LTA zeolites (Si/Al = 16–23) have significantly better hydrothermal stability than Cu/SSZ-13 in $NH_3$-SCR reactions, especially under harsh hydrothermal aging temperature (e.g., 900 °C), where Cu/LTA zeolites maintain remarkable NO reduction activities [25].

Overall, previous studies have shown that Cu/LTA exhibits outstanding hydrothermal stability for standard $NH_3$-SCR. However, the Cu/LTA hydrothermal stability mechanism remains unclear, and this is the main purpose of our current study. Also, to the best of our knowledge, the effect of aging of Cu/LTA for fast $NH_3$-SCR reaction, and for examining ammonium nitrate formation, is also done for the first time in this work. To investigate the effect of hydrothermal aging on Cu/LTA, the hydrothermal treatment was conducted at 800 °C, 850 °C and 900 °C, respectively and compared with a sample degreened at 750 °C. The influence on the zeolite structure, acidity and the nature of Cu species is examined using a broad range of techniques, such as flow reactor experiments, in situ DRIFT spectroscopy, $H_2$ TPR, BET, XRD and solid-state NMR.

## 2. Experimental section

### 2.1. Catalyst synthesis

LTA (Si/Al = 15) was hydrothermally synthesized in-house using a method reported by Jo et al. [24] with small modifications. For Organic Structure-Directing Agent (OSDA) synthesis, details are as follows: 9.6 g 1,2-dimethyl imidazole (98%, Aldrich), 14.6 g 4-methylbenzyl chloride (98%, Aldrich) and 100 ml chloroform (99%, Aldrich) were charged into a 250 ml beaker and stirred for two days at room temperature. The final solid/solution mixture was dried through rotary evaporation at 80 °C for 1 h. The obtained OSDA was converted to hydroxide form using Amberlite IRN-78 anion-exchange resin (Aldrich) with the feed ratio of 10 g of OSDA and 150 ml of resin in 200 ml deionized water stirring for 3 h at room temperature. The resulting solution was concentrated with rotary evaporation at 80 °C, and the hydroxide form OSDA was titrated using 0.1 M HCl with phenolphthalein as the indicator. After that, for zeolite synthesis, composition of the gel was as follows: 15OSDA: 2TMAOH: 15HF: $30SiO_2$: $1Al_2O_3$: $150H_2O$. The gel was prepared by first dissolving tetramethylammonium hydroxide pentahydrate ($TMAOH{\cdot}5H_2O$, 97%, Aldrich) in the OSDA solution. Following this, $Al(OH)_3$ (containing 54% $Al_2O_3$, Aldrich) and tetraethylorthosilicate (TEOS, 98%, Aldrich) were added sequentially under stirring for 24 h. Then, the ethanol formed from TEOS hydrolysis and excess water were evaporated through heating at 80 °C. Thereafter, the desired amount of HF acid was added dropwise. Finally, the mixture was sealed into a 160 ml Teflon-lined stainless-steel autoclave. The autoclave was placed in a sand bath on top of a hot plate stirrer to carry out hydrothermal synthesis at 175 °C for 96 h under continuous stirring (100 rpm). After synthesis, the product was separated from the mother liquid via filtration and washed with deionized water. Finally, the as-made zeolite was dried at 100 °C in the oven over night and calcined at 600 °C for 8 h in the static air to remove the OSDA.

Cu/LTA was prepared using the incipient wetness impregnation (IWI) method. The conventional methods to introduce copper species into zeolites (e.g., SSZ-13) is solution ion-exchange and solid-state ion-exchange (SSIE), which may be facilitated by gas phase treatment (e.g., $NH_3$, NO, $H_2O$) [26]. The advantages of IWI including that: (1) it is easier to regulate the loading of Cu in comparison with the traditional solution ion-exchange method and (2) it may also be beneficial for the dispersion of Cu species compared to SSIE. In this work the Cu/LTA was prepared with IWI method reported previously [27], which is modified slightly from the protocol developed by Shishkin et al. [28]. First, 0.180 g of $Cu(NO_3)_2{\cdot}2.5H_2O$ was added into 3 ml of ethanol with stirring until completely dissolved. 2 g of LTA zeolite was slowly introduced into the solution, then the mixture vessel was capped and stirred for 15 min. After that, the product was dried at room temperature overnight in the fume hood.

The as-prepared powder was first calcined at 600 °C for 8 h, then ramped up to 750 °C for 2 h. The calcined powder was used to coat a monolith (400 cpsi) with 15 mm diameter and 20 mm length. The details of the washcoat procedure can be found in our prior work [29]. To increase the attachment of the zeolite, alumina (Disperal P2, Sasol) was used as a binder when coating the zeolite, with a ratio 95/5 between zeolite and binder. The total washcoat weight was ~280 mg. The prepared monolith was then calcined at 500 °C for 2 h. Prior to use, the monolith was first degreened at 750 °C for 4 h in the reaction condition (400 ppm NO, 400 ppm $NH_3$, 5% $H_2O$, 8% $O_2$, 1200 ml/min), denoted as Cu/LTA-750. Also, the monolith was further hydrothermal aged at 800, 850 °C for 10 h and 900 °C for 8 h, respectively, in 21% $O_2$, 10% $H_2O$ in Ar, denoted as Cu/LTA-800, Cu/LTA-850 and Cu/LTA-900, respectively. The reason for using such high temperature for degreeening was to facilitate the movement of copper species into ion-exchanged positions, since incipient wetness impregnation was used for copper addition. Indeed, the color shifts from slightly grayish to blue after degreening, indicating copper transfer to ion-exchange positions. Moreover, STEM images (not shown here) for Cu/LTA-750 and Cu/LTA-900 did not show any signs of copper particles. The analysis of Cu, Si, Al elements, determined with inductively coupled plasma atomic emission spectroscopy (ICP-AES), was conducted at ALS Scandinavia AB. Cu loadings, Si/Al, Cu/Al ratios of the catalyst are displayed in Table 1.

### 2.2. Catalyst characterization

Powder X-Ray diffraction (XRD) measurements of the catalysts were performed in a SIEMENS diffractometer D5000 operating at 40 kV and 40 mA with Cu Kα radiation (λ = 1.5418 Å). Data were collected with 2θ ranging from 5° to 50° using a step size of 0.02. SEM images were acquired using an FEI Quanta 200 ESEM (Environmental SEM) coupled with an Oxford X-max 80 EDX detector.

A Tristar 3000 (Micromeritics) instrument was used to measure the $N_2$ adsorption and desorption isotherms at 77 K. Before the measurements, all catalysts were outgassed at 250 °C for 10 h under flowing $N_2$. The Brunauer-Emmett-Teller (BET) method was used to calculate the specific surface areas. Pore volume was obtained using the Barrett-Joyner-Halenda (BJH) method.

$^{27}Al$ solid-state NMR experiments were carried out on a Bruker Avance III 500 MHz spectrometer equipped with a 4 mm HX CP MAS probe. Experiments were recorded at a magic angle spinning rate of 11 kHz and the temperature was set to 298 K. The $^{27}Al$ ppm scale was referenced externally to the $^{13}C$ chemical shift of adamantane. The repetition delay was set to 2 s and a 20° radio frequency pulse was used for excitation. The signal was accumulated 800 times and normalized by the sample weight packed in the rotor.

In situ Diffuse Reflectance Infrared Fourier Transform Spectra (DRIFTS) were acquired with a Bruker Vertex 70 spectrometer,

**Table 1**
ICP-AES results of the Cu/LTA sample.

| sample | Si content (wt.%) | Al content (wt.%) | Cu content (wt.%) | Si/Al ratio | Cu/Al ratio |
|---|---|---|---|---|---|
| Cu/LTA | 37.9 | 2.46 | 2.32 | 15.0 | 0.4 |

equipped with an MCT detector and operated at 4 $cm^{-1}$ resolution. Each spectrum reported is obtained by averaging 256 scans. Prior to each measurement, the catalysts were heated in 100 ml/min 10 vol.% $O_2$/Ar to 500 °C, held at this temperature for 1 h to remove impurities. For the study of $[Cu(OH)]^+$ and $Cu^{2+}$ through framework internal asymmetric T-O-T vibrations, the catalysts were cooled to 200 °C to carry out the adsorption of $NH_3$ (300 ppm $NH_3$, 10 vol.% $O_2$, balance Ar) until saturation. Subsequently, the catalyst was purged in 10 vol.% $O_2$/Ar for 20 min, then followed by NO (300 ppm NO, 10 vol.% $O_2$, balance Ar) for an exposure of 3 h. The spectra were recorded as a function of time using the background measured at 200 °C in a flow of 10 vol.%$O_2$/Ar.

$H_2$-temperature programmed reduction ($H_2$-TPR) of the catalysts were performed on a Differential Scanning Calorimeter (Sensys DSC, Setaram), connected with a mass spectrometer (Hiden HPR-20 QUI MS) to detect the outlet gases. Measurements were conducted on both fully hydrated samples, and dehydrated samples pretreated in flowing air (21% $O_2$ in Ar) at 500 °C for 1 h and then cooled to ambient temperature prior to TPR. TPR was conducted from ambient temperature to 800 °C at 10 °C/min in 0.2% $H_2$/Ar.

$NH_3$ temperature-programmed desorption ($NH_3$-TPD) was used to measure $NH_3$ adsorption on Lewis and Brønsted acid sites in the catalysts. $NH_3$-TPD was carried out using the SCR reactor system, with $NH_3$ detection via an online MKS 2030 FTIR analyzer. The same monoliths (~280 mg catalyst) used previously for SCR reactions (see Section 2.3) were used for $NH_3$-TPD measurement, and the experimental steps were as follows: (1) heat the sample to 550 °C in $O_2$/Ar (1200 ml/min, 10% $O_2$, 5% $H_2O$) and keep at 550 °C for 30 min; (2) stop $O_2$ flow, maintain Ar flow with 5% $H_2O$, and cool sample to $NH_3$ adsorption temperatures of 100 °C; (3) adsorb $NH_3$ (400 ppm in Ar, 5% $H_2O$) until outlet $NH_3$ concentrations remain constant for 1 h; (4) turn off the $NH_3$ flow and purge with Ar with 5% $H_2O$ for 20 min at the adsorption temperature; and (5) ramp from the adsorption temperature to 600 °C at 20 °C /min, and maintain at 600 °C for 20 min while measuring $NH_3$ concentrations in the outlet.

For XRD, BET, $^{27}Al$ solid-state NMR and $H_2$-TPR powder catalyst was used, which had been degreened/aged in a crucible in the flow reactor, as described in Section 2.3.

### 2.3. Reaction tests

All the activity experiments and the hydrothermal aging were performed on washcoated monoliths in a flow reactor. Details about the reaction system can be found in our previous publications [27]. Briefly, the reactor consists of a quartz tube, where the temperature is measured about 1 cm before the catalyst and also in the center of one channel. The temperatures given in this paper refers to the gas phase temperature about 1 cm before the catalyst. The gases were mixed using several Bronkhorst MFC and the water was added with Bronkhorst CEM system. Concentrations of reactants and products were measured with the online MKS 2030 FTIR analyzer. For standard SCR ($4NO + 4NH_3 + O_2 \rightarrow 4N_2 + 6H_2O$), the feed gas contained 400 ppm NO, 400 ppm $NH_3$, 10% $O_2$, 5% $H_2O$ and balance Ar. For fast SCR ($NO + NO_2 + 2NH_3 \rightarrow 2N_2 + 3H_2O$), 400 ppm NO was replaced by 200 ppm NO and 200 ppm $NO_2$, the other feed was same as above. For $NH_3$ or NO oxidation, NO or $NH_3$ was not included in the feed gas while others maintained the same. Measurements were conducted from high to low reaction temperatures, and monoliths were maintained at each target temperature for 30 min. The temperature-programmed desorption (TPD) measurements after fast SCR were conducted by linearly heating the monoliths from 150 °C to 550 °C, while exposing the catalyst to only Ar. Prior to all experiments, the catalyst was pre-treated with 21% $O_2$ in Ar at 550 °C for 20 min. All the gas lines were maintained above 100 °C to avoid water condensation. The total gas flow was 1200 sccm, and the gas hourly space velocity (GHSV) was estimated to be 22,100 $h^{-1}$ for the monolith (a catalyst amount of ~280 mg).

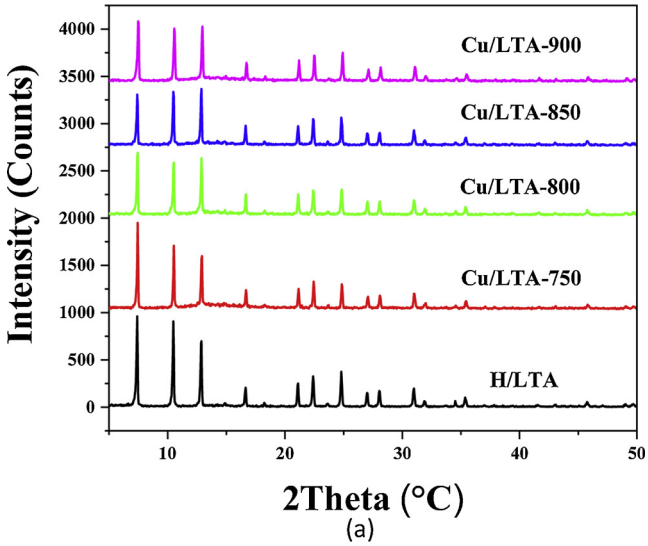


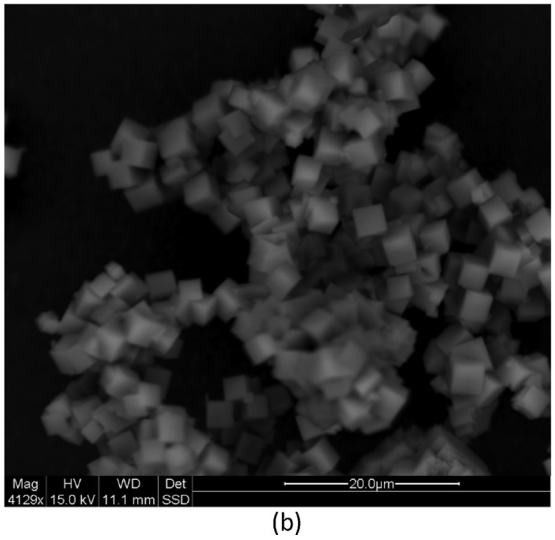


**Fig. 1.** (a) XRD patterns of the H/LTA and Cu/LTA hydrothermally aged at different temperatures, (b) SEM image of H/LTA sample.

## 3. Results and discussion

### 3.1. Characterization results

As shown in the XRD measurements presented in Fig. 1(a), the structure of the aged Cu/LTA catalysts is well maintained, even after hydrothermal aging at 900 °C for 8 h in the presence of 10% $H_2O$ and 21% $O_2$. Fig. 1(b) presents the SEM image of pure H/LTA synthesized in this study. The crystal morphology of LTA was found to be uniform cubic with an average size of ~3 μm. Moreover, Table 2 displays BET surface areas and pore volumes of H/LTA and aged Cu/LTA catalysts. Only minor changes can be observed for samples upon aging. For

**Table 2**
BET surface areas, pore volumes for H/LTA and Cu/LTA hydrothermally aged at different temperatures.

| sample | BET surface area ($m^2$/g) | Pore volume ($cm^3$/g) |
|---|---|---|
| H/LTA | 570 | 0.298 |
| Cu/LTA-750 | 542 | 0.281 |
| Cu/LTA-800 | 530 | 0.277 |
| Cu/LTA-850 | 513 | 0.263 |
| Cu/LTA-900 | 495 | 0.251 |

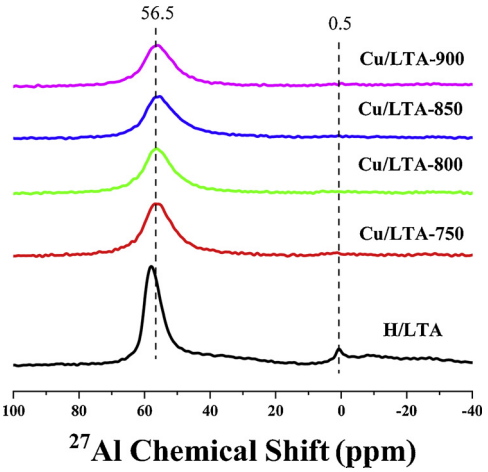


**Fig. 2.** $^{27}$Al solid state NMR of H/LTA and Cu/LTA hydrothermally aged at different temperatures.

instance, in comparison with Cu/LTA-750, less than 10% of surface area loss when aging temperature goes up to 900 °C. These results show the incredible stability of Cu/LTA, which is in line with the study by Ryu et al. [25].

Unlike XRD and BET, $^{27}$Al-NMR is highly sensitive to subtle changes in the local Al environment during aging [30]. Fig. 2 presents $^{27}$Al spectra for H/LTA and aged Cu/LTA catalysts under ambient condition. The $^{27}$Al spectrum for fresh H/LTA exhibits resonances at approximately 56.5 and 0.5 ppm which is corresponding to tetrahedrally coordinated framework Al and extra-framework octahedral Al, respectively [11,31]. Notably, the extra-framework Al (0.5 ppm) becomes invisible in all Cu/LTA catalysts. As the samples are synthesized using IWI method, it is not possible to remove these extra-framework Al during the solution ion-exchange step with the help of water as mentioned in the literature for Cu/SSZ-13 synthesis [30]. Moreover, comparing with H/LTA, a decrease in intensity of tetrahedral Al of ca 20% is observed for all degreened/aged Cu/LTA catalysts (e.g., Cu/LTA-750). It should be noted that in Cu/zeolites, paramagnetic centers (i.e. $Cu^{2+}$) located close to tetrahedral Al can also cause the loss of signal [16]. Our results from BET and XRD suggest a small amount of dealumination between H/LTA and Cu/LTA, consequently the paramagnetic $Cu^{2+}$ sites cause signal loss. However, when increasing the aging temperature, such as from Cu/LTA-750 to Cu/LTA-800, the loss in signal is only a few percent, which indicates that only a small amount of dealumination occurs. These results clearly show the exceptional hydrothermal stability of the LTA structure even up to 900 °C.

Previous studies have shown that different types of Cu species may simultaneously exist in Cu/zeolites: $Cu^{2+}$ ions with two neighboring framework Al providing two negative framework charges (Z2Cu), $[Cu(OH)]^+$ with one framework Al needed for one negative framework charge (ZCuOH), and small $CuO_x$ clusters in the cages [32–35]. The nature and quantity of Cu species are influenced by multiple factors including zeolites structure, Si/Al ratios, Cu loadings and preparation methods. As $Cu^{2+}$ and $[Cu(OH)]^+$ have different binding energies with the zeolite framework, it is possible to detect such differences using $H_2$-TPR, in terms of the different reduction temperatures, which has been done in multiple studies [36–38].

One additional sample, i.e. fresh Cu/LTA (Si/Al = 15) with Cu/Al ~0.2, prepared with solution ion-exchange method was used to examine the mentioned reduction peaks, for both hydrated and dehydrated samples using $H_2$-TPR. The detailed preparation method can be found in the Supporting information (SI). Considering the relatively low Cu loading and the preparation method for this sample, the possibility of the presence of $CuO_x$ clusters is quite low. Hence, the reducible Cu species should be only $Cu^{2+}$ and $[Cu(OH)]^+$ at temperatures below 600 °C, as $Cu^+$ is normally reduced above this temperature [39]. As displayed in Fig. S-1(a) (see Supporting information), the hydrated sample displays two reduction peaks centered at ~280 °C and ~480 °C. $[Cu(OH)]^+$ is expected to show a lower temperature reduction peak since the binding energy with the framework of $[Cu(OH)]^+$ is lower than that of $Cu^{2+}$. Based on this, the reduction peak at ~280 °C could be assigned to the reduction of $[Cu(OH)]^+$, while the higher temperature

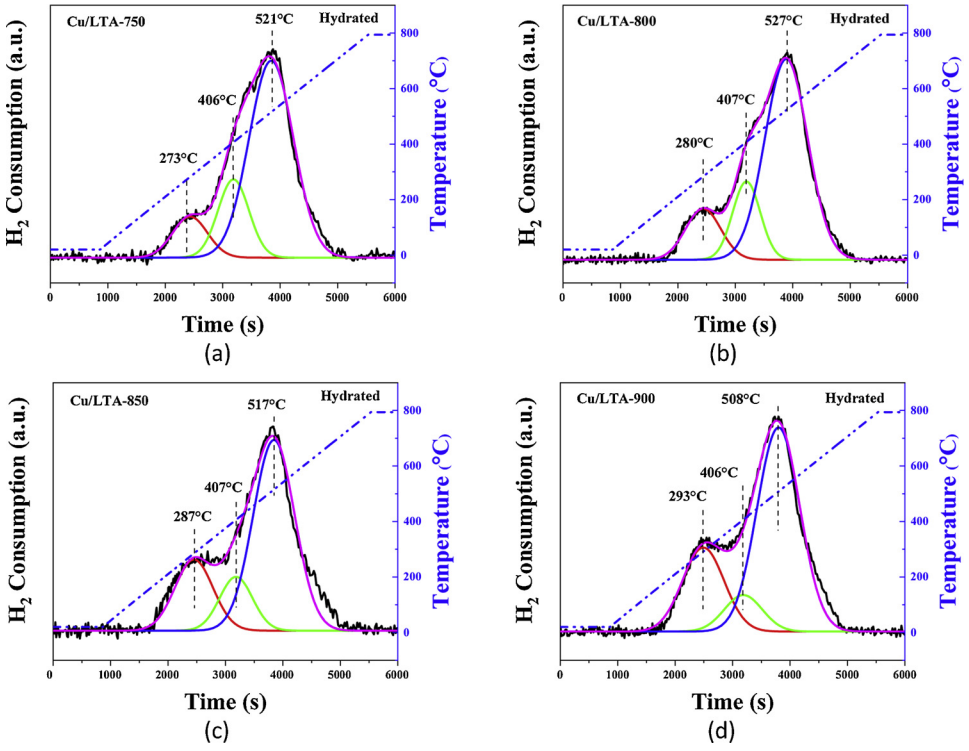


**Fig. 3.** $H_2$-TPR curves for the ambient (hydrated) (a) Cu/LTA-750, (b) Cu/LTA-800, (c) Cu/LTA-850 and (d) Cu/LTA-900 samples.

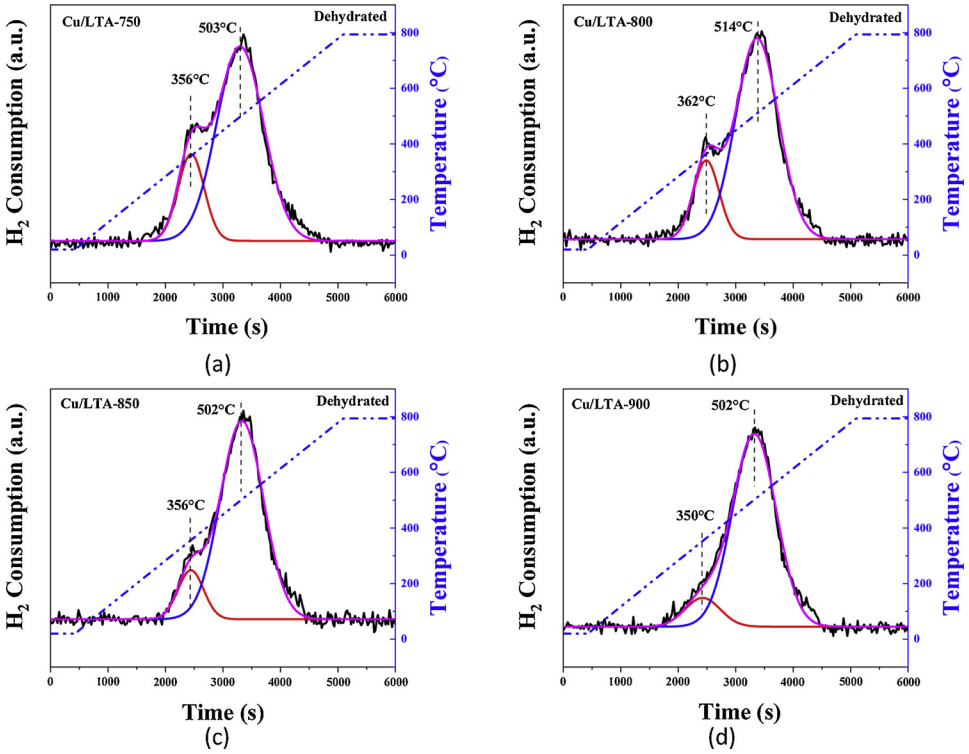


**Fig. 4.** $H_2$-TPR curves for the pretreated (dehydrated) (a) Cu/LTA-750, (b) Cu/LTA-800, (c) Cu/LTA-850 and (d) Cu/LTA-900 samples.

peak (~480 °C) is contributed from the reduction of $Cu^{2+}$ (Z2Cu). Also it could possibly be due to some partially dehydrated $[Cu(OH)]^+$ present prior to reduction, which will be discussed later. Fig. S-1(b) presents the result for the dehydrated sample (which was pretreated in 21% $O_2$ in Ar at 500 °C for 1 h), and only a single dominant reduction peak at ~440 °C can be found which is assigned to the reduction of both $Cu^{2+}$ and $[Cu(OH)]^+$ simultaneously. This indicates the difference of reduction behavior between $Cu^{2+}$ and $[Cu(OH)]^+$ disappears after removing the $H_2O$ from Cu/LTA cages, which this is not the case for Cu/SSZ-13 where both reduction peaks remain [40].

Figs. 3 and 4 present the $H_2$-TPR results of the ambient (hydrated) and pretreated (dehydrated) Cu/LTA samples that are hydrothermally aged at different temperatures. The hydrated samples display two distinct reduction peaks centered at ~280 °C and ~520 °C and one apparent shoulder located at ~410 °C. In contrast, the $H_2$-TPR curves for dehydrated samples are simpler as displayed in Fig. 4 with only two reduction peaks located at ~360 °C and ~510 °C, respectively. Based on the results for $H_2$-TPR for Cu/LTA (Cu/Al = 0.2) discussed above, we assign the ~280 °C (hydrated samples) to reduction of $[Cu(OH)]^+$ and ~520 °C (hydrated samples) reduction peak mainly due to reduction of $Cu^{2+}$ and possibly due to a portion of dehydrated $[Cu(OH)]^+$ prior to reduction, which will be discussed later. The reduction shoulder at ~410 °C (hydrated samples) most likely reflects the reduction from $CuO_x$ clusters in the samples. Since the IWI preparation method, used in this study has similarities to solid state ion-exchange method, it is not unexpected to reveal certain amount of $CuO_x$ clusters. Next, for dehydrated samples, the reduction peak (at ~510 °C) is attributed to the reduction of both $Cu^{2+}$ and $[Cu(OH)]^+$ (refer Fig. S-1(b)) and the peak at ~360 °C should still be due to $CuO_x$ clusters.

For an in-depth understanding of hydrothermal aging and its impact on the distribution of Cu species in the Cu/LTA samples, the method of peak deconvolution is applied to quantify $Cu^{2+}$, $[Cu(OH)]^+$ and $CuO_x$ species according to the relative peak areas in both hydrated and dehydrated TPR profiles. Table 3 lists the populations of different Cu species from $H_2$-TPR for Cu/LTA hydrothermally aged at different temperatures. First, it can be easily seen that the populations of $CuO_x$ clusters are quite identical in the hydrated and dehydrated profiles. For example, in Cu/LTA-750 the hydrated TPR contains 10.6% $CuO_x$ clusters and 11.0% for the dehydrated ones and for Cu/LTA-900 samples the corresponding values are 5.5% and 5.6%, respectively. This also indirectly confirms that these two reduction peaks (410 °C for hydrated, 360 °C for dehydrated) correspond to the same Cu species, i.e. $CuO_x$ clusters. Moreover, the amount of $CuO_x$ clusters are quite low, which is consistent with STEM images (data not shown), where no copper particles were visible for Cu/LTA-750 and Cu/LTA-900 samples. From Table 3, it is also worth noting that when increasing the hydrothermal aging temperature, the $[Cu(OH)]^+$ population increases, along with a drop of both $CuO_x$ and $Cu^{2+}$ contents. The possible reaction can be described as follows:

$$Z\text{-}Cu^{2+}\text{-}Z + Cu_xO_y + H_2O = 2\ Z\text{-}[Cu(OH)]^+ + Cu_{x-1}O_{y-1} \quad (1)$$

$$Z\text{-}Cu^{2+}\text{-}Z + H_2O = Z\text{-}[Cu(OH)]^+ + Z\text{-}H \quad (2)$$

$$Z\text{-}H + Cu_xO_y = Z\text{-}[Cu(OH)]^+ + Cu_{x-1}O_{y-1} \quad (3)$$

Reaction (1) suggests that when certain $CuO_x$ clusters are close to the isolated $Cu^{2+}$ ions with two framework Al nearby, upon aging, one copper atom from $CuO_x$ may compete with isolated $Cu^{2+}$ ions, resulting in the formation of two $[Cu(OH)]^+$. Moreover, Reactions (2) and (3) are also the possible pathways when no isolated $Cu^{2+}$ ions and $CuO_x$ are close to each other. Interestingly, this phenomenon is not observed for Cu/SSZ-13, where we earlier found more $CuO_x$ clusters with increasing aging temperature [17]. Moreover, Gao et al. [1] showed for Cu/SSZ-13 that with increasing aging temperature, $[Cu(OH)]^+$ content monotonically decreased, while $CuO_x$ content gradually increased and that the $Cu^{2+}$ content first increased and then become stable at higher aging temperatures. Notably, the formation of $CuO_x$ clusters, mostly from $[Cu(OH)]^+$ in Cu/SSZ-13 during hydrothermal aging is primarily responsible for the high-temperature selectivity loss, catalyst deactivation and structure collapse [1,41]. However, $H_2$-TPR results indicate that $[Cu(OH)]^+$ is more stable in Cu/LTA samples from this study, even after harsh aging at 900 °C for 8 h.

Recent studies indicated that $Cu^{2+}$ and $[Cu(OH)]^+$ can be clearly

**Table 3**
Populations of different Cu species from $H_2$-TPR for Cu/LTA hydrothermally aged at different temperatures.

| sample | | hydrated | | dehydrated | |
|---|---|---|---|---|---|
| | $[Cu(OH)]^+/Cu_{all}$ (%) | $CuO_x/Cu_{all}$[a] (%) | $Cu^{2+}/Cu_{all}$ (%) | $CuO_x/Cu_{all}$ (%) | $([Cu(OH)]^+ + Cu^{2+})/Cu_{all}$ (%) |
| Cu/LTA-750 | 12.5 | 10.6 | 76.9 | 11.0 | 89.0 |
| Cu/LTA-800 | 15.6 | 9.4 | 75.0 | 9.8 | 90.2 |
| Cu/LTA-850 | 23.5 | 7.7 | 68.8 | 7.2 | 92.8 |
| Cu/LTA-900 | 27.3 | 5.5 | 67.2 | 5.6 | 94.4 |

[a] $CuO_x/Cu_{all}$ = 1/2Reduction Peak Area $_{CuOx}$/(Reduction Peak Area$[Cu(OH)]^+$ + 1/2 Reduction Peak Area$_{CuOx}$ + Reduction Peak Area$Cu^{2+}$).

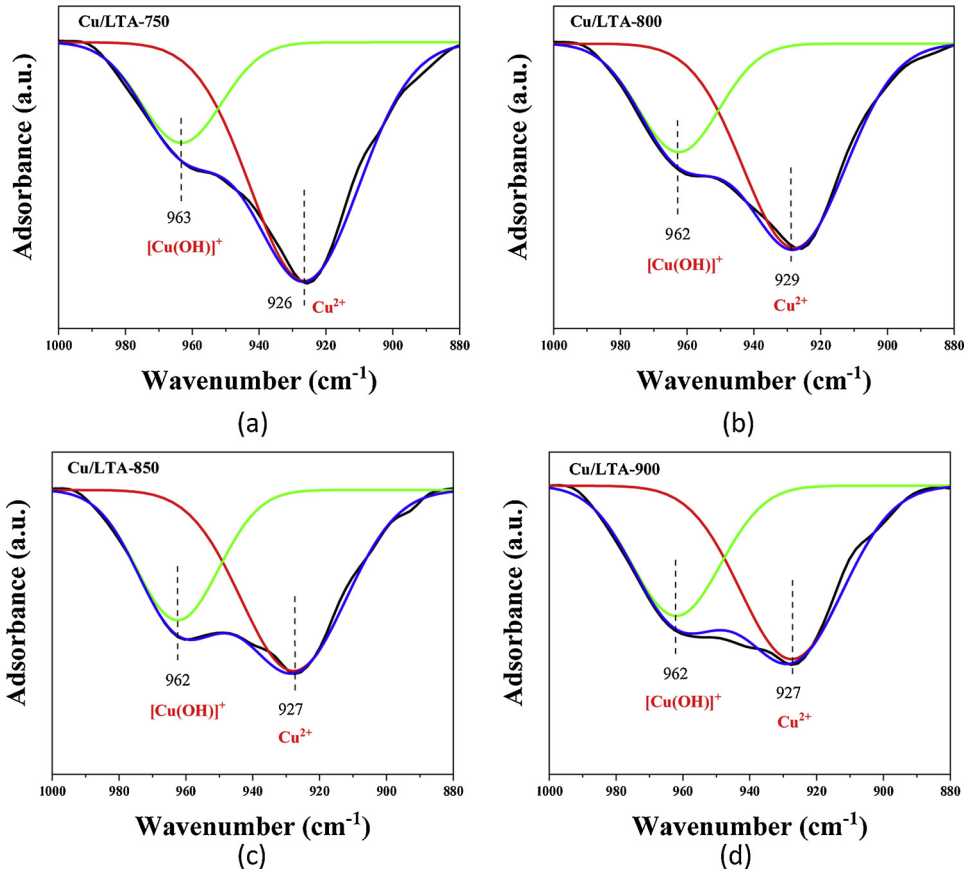


**Fig. 5.** DRIFTS spectra of T-O-T vibrational region perturbed by $NH_3$ adsorption for (a) Cu/LTA-750, (b) Cu/LTA-800, (c) Cu/LTA-850 and (d) Cu/LTA-900 samples.

distinguished in Cu/SSZ-13. This is based on the perturbation to asymmetric T-O-T vibrations of the zeolite framework, with the IR features at ~900 and ~950 $cm^{-1}$ respectively [37,42]. Luo et al. [43] found that with the help of $NH_3$, by taking spectra in $NH_3$-saturated samples using $NH_3$-free dehydrated forms as background, a much better-resolved, negative perturbed T-O-T vibrations IR signals can be obtained. So in this work we apply the same protocol also for Cu/LTA. Therefore, to further investigate the effect of hydrothermal aging and to examine the stability of $[Cu(OH)]^+$, in situ DRIFTS of $NH_3$ adsorption was measured and shown in Fig. 5 and the DRIFTS spectra for each sample during $NH_3$ adsorption over time can be found in Fig. S-2. It should be noted that the baseline subtraction is performed for all the spectra from DRIFTS. For all four Cu/LTA samples degreened/aged at different temperatures, two well-resolved negative bands centered at ~930 and ~960 $cm^{-1}$ are clearly visible which are corresponding to $Cu^{2+}$ and $[Cu(OH)]^+$, respectively. In a comparison with Cu/SSZ-13, the Cu/LTA exhibits a shift of the IR signals to higher wavenumbers, i.e. 926 and 962 $cm^{-1}$ for Cu/LTA and ~900 and ~950 $cm^{-1}$ for Cu/SSZ-13 [37,42]. The reason for this is suggested to be: (1) the framework structures of LTA and SSZ-13 are different, and/or (2) the Cu/LTA samples used in the present study have already been degreened/hydrothermally aged, whereas for Cu/SSZ-13, the ~900 $cm^{-1}$ band is also found to shift to ~920 $cm^{-1}$ after aging above 650 °C [1].

The evolution of these two Cu species with aging are examined and we observe that the relative intensity of the band ~930 $cm^{-1}$ decreases gradually with the synchronous increase of the one at ~960 $cm^{-1}$ suggesting that a portion of $Cu^{2+}$ is progressively converted to $[Cu(OH)]^+$ upon aging. These results are consistent with $H_2$-TPR profiles displayed in Fig. 3. This further emphasizes the unusual stability of $[Cu(OH)]^+$ in the Cu/LTA catalysts samples reported in this study. For a more intuitive and clear understanding of the changes in $Cu^{2+}$ and $[Cu(OH)]^+$ with increasing aging temperature, peak fittings are used to calculate the area ratios of $Cu^{2+}$ and $[Cu(OH)]^+$ for all samples. Thereafter the results are plotted in Fig. 6, together with the $H_2$-TPR results obtained from Fig. 3 for comparison. The trend of $Cu^{2+}$ and $[Cu(OH)]^+$ populations with increasing aging temperature from both $H_2$-TPR and DRIFTS is completely identical. The only difference is that the content of $[Cu(OH)]^+$ is lower from $H_2$-TPR results through all samples. A possible explanation is that $[Cu(OH)]^+$ is partially dehydrated prior to reduction, as mentioned above, indicating that the reduction of [Cu

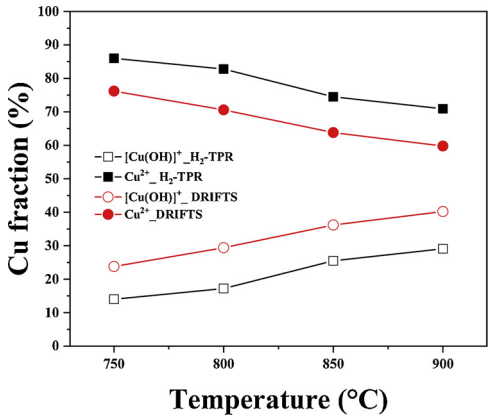


**Fig. 6.** $[Cu(OH)]^+$ and $Cu^{2+}$ populations for Cu/LTA hydrothermally aged at different temperatures quantified using DRIFTS and $H_2$-TPR.

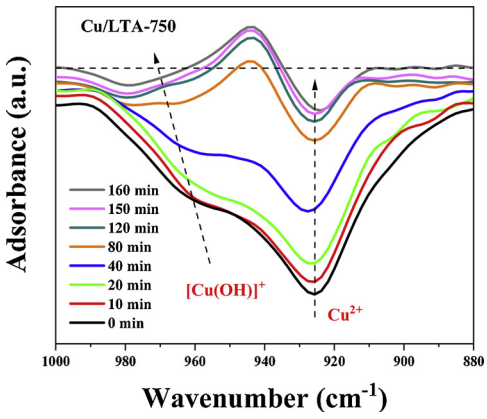


**Fig. 8.** DRIFTS spectra of T-O-T vibrational region with 300 ppm NO feeding to react with preadsorbed $NH_3$ over time.

$(OH)]^+$ species may also have contributed to the reduction peak at ~520 °C (Fig. 3).

In addition to the interesting finding concerning $Cu^{2+}$ and $[Cu(OH)]^+$ from $NH_3$ adsorption, the OH vibrational information is also available. A few negative bands at 3734, 3707, 3672, 3648, 3615 and 3562 $cm^{-1}$ are observed in Fig. 7. The bands at 3734 and 3672 $cm^{-1}$ are assigned to $NH_3$ adsorbed on the external Si−OH and Al−OH sites respectively [1,44]. The 3615 and 3562 $cm^{-1}$ bands are normally attribute to the Al-OH-Si, in other words, Brønsted acid sites [45,46]. The band at 3648 $cm^{-1}$ is most possibly attributed to the Cu−OH species [47]. The signal at 3707 $cm^{-1}$ is not clear and may need further investigation. Interestingly, the intensities of 3615 and 3562 $cm^{-1}$ bands are relatively stable and only exhibit a slight decrease with an increase in hydrothermal aging temperatures. This suggests that most of the Brønsted acid sites survived, even after harsh aging at 900 °C. This is another remarkable feature of Cu/LTA, because other zeolites, such as Cu/SSZ-13 and Cu/BEA, quickly lose the Brønsted acid sites upon hydrothermal aging [17,48]. Our results also indicate that the degree of dealumination is quite low in the aged Cu/LTA samples, which is consistent with the $^{27}Al$ NMR results (see Fig. 2).

Following the $NH_3$ adsorption (300 ppm $NH_3$, 10 vol.% $O_2$, balance Ar) and then Ar purge for 20 min, NO (300 ppm NO, 10 vol.% $O_2$, balance Ar) was added into the feed gas to react with $NH_3$ preadsorbed by the Cu(II) species (i.e., $Cu^{2+}$ and $[Cu(OH)]^+$). Fig. 8 depicts the DRIFTS spectra obtained during the reaction between NO and preadsorbed $NH_3$ at 200 °C for Cu/LTA-750. The results for other samples can be found in Fig. S-3. It can be clearly observed that when 300 ppm NO passes over the sample, the surface $NH_3$ is consumed gradually over time and the negative IR features at 930 and 960 $cm^{-1}$ move towards the baseline. This confirms that both $[Cu(OH)]^+$ and $Cu^{2+}$ are active for the $NH_3$-SCR reaction at 200 °C. However, even after flowing the feed of NO for nearly 3 h, small negative bands still exist, which is not the case for Cu/SSZ-13, where 500 ppm NO only needed 20 min to completely react with adsorbed $NH_3$ at 200 °C with a flow rate of 50 sccm [38]. This could be due to either: (1) a portion of the Cu(II) species is less active for ammonia SCR, or (2) location of some Cu(II) species, that are not accessible for NO after $NH_3$ adsorption, possibly due to sterical hindrance.

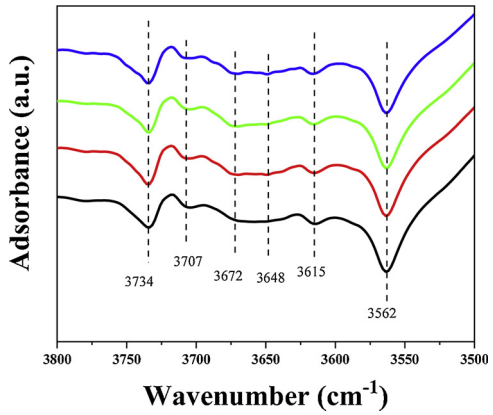


**Fig. 7.** DRIFTS spectra of OH vibrational region by $NH_3$ adsorption for Cu/LTA-750(black), Cu/LTA-800(red), Cu/LTA-850(green) and Cu/LTA-900 samples (blue) (For interpretation of the references to colour in this figure legend, the reader is referred to the web version of this article).

The results from $NH_3$-TPD for Cu/LTA samples hydrothermally aged at different temperatures are shown in Fig. 9(a). Initially (6–8 min), no $NH_3$ is observed due to the complete storage of $NH_3$ in the Cu/LTA samples. $NH_3$ then breaks through and reaches the feeding concentration (400 ppm) over the course of a few minutes. The $NH_3$ storage is larger for the Cu/LTA with lower hydrothermal aging temperatures, which can be observed by both longer adsorption time and the quantity of the $NH_3$ desorbed. Further, when the $NH_3$ feeding is turned off, weakly adsorbed $NH_3$ is generally purged out with the inert gas. As the temperature rises, the desorption of $NH_3$ can be clearly observed and the enlarged curves are presented in Fig. 9(b). In order to facilitate the interpretation of the Cu/LTA samples, an $NH_3$-TPD was conducted over fresh H/LTA sample and the results are displayed in Fig. S-4. Two $NH_3$ desorption peaks are observed for the H/LTA sample, centered at ~190 °C and ~340 °C and in addition some ammonia is released already during flushing of the sample. The low temperature peak, and ammonia released during flushing, can be assigned to $NH_3$ desorption from weak acid sites. For example, external Si−OH and Al−OH, which are observed from DRIFTS and the high temperature peak is attributed to the desorption of $NH_3$ from Brønsted acid sites, i.e. Al-OH-Si [49].

Analysis of $NH_3$-TPD results for Cu/LTA samples display two apparent desorption peaks located at ~230 °C and ~315 °C. In addition, the amount of stored/desorbed ammonia is significantly larger for Cu/LTA than for H/LTA, where both the high temperature peak as well as the low temperature peak are increasing. For H/LTA the peak at ~190 °C is ca 80 ppm, while the peak at ~230 °C for Cu/LTA-750 is ca 230 ppm. The corresponding high temperature peaks are 200 ppm at ~340 °C for H/LTA and 280 ppm at ~315 °C for Cu/LTA-750, respectively. These findings indicate that both peaks are likely a combination of ammonia stored both on the zeolite as well as the copper sites, which is in agreement with our earlier results for H/SSZ-13 and Cu/SSZ-13, although the peak temperatures are different [50]. However, the peak at 230 °C for Cu/LTA is significantly larger compared to the peak at 190 °C for H/LTA, indicating that most of the peak is likely contributed by the desorption of $NH_3$ from $Cu^{2+}$ and $[Cu(OH)]^+$ sites. Furthermore, the high temperature peak can mostly be assigned to the $NH_3$ desorption

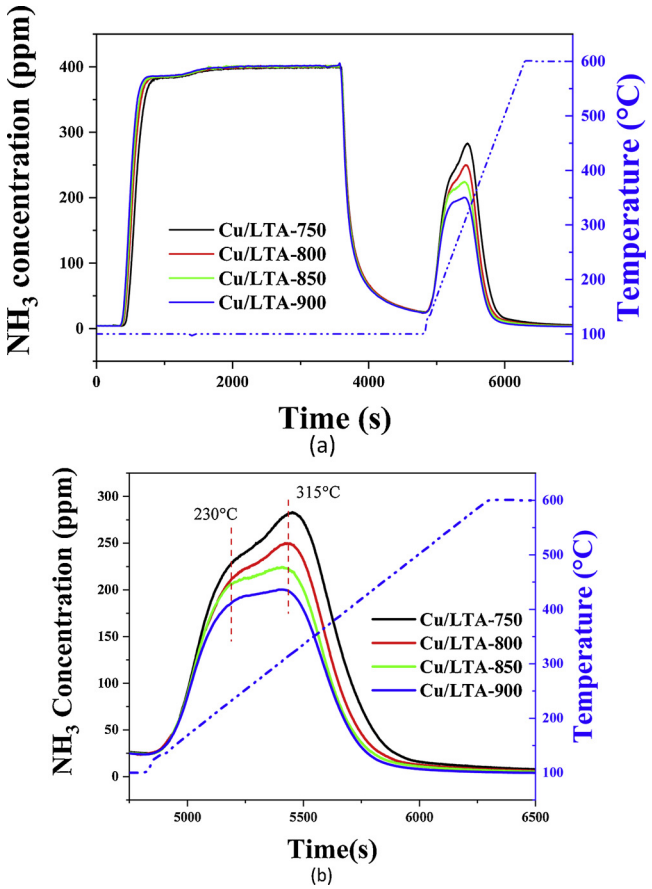


**Fig. 9.** $NH_3$-TPD profiles for Cu/LTA hydrothermally aged at different temperatures (a) both adsorption and desorption regions and (b) desorption region.

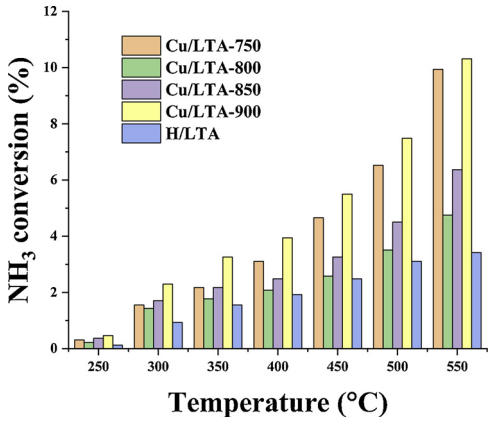


**Fig. 10.** $NH_3$ conversion as a function of temperature during $NH_3$ oxidation for H/LTA and Cu/LTA hydrothermally aged at different temperatures. The reactant feed contained 400 ppm $NH_3$, 10% $O_2$, 5% $H_2O$ balanced with Ar at a GHSV of 22,100 $h^{-1}$.

from Brønsted acid sites [51], but also some contribution from ammonia stored on copper is observed. For the Cu/LTA sample there is a large desorption of ammonia during flushing of the sample, which can be assigned to $NH_3$ desorption from weak acid sites, e.g. Si−OH and Al−OH, as well as weakly adsorbed ammonia on copper sites, since the desorption during flushing is higher for Cu/LTA than H/LTA. These results are consistent with our previous experimental and modelling studies for Cu/SSZ-13 [52]. These results are also in line with the DRIFTS spectra shown in Fig. 7, where the Si−OH and Al−OH vibration can be clearly observed.

During hydrothermal aging, the desorption of $NH_3$ from both Brønsted acid sites and Cu(II) species decreases to some extent. The decrease in Brønsted acid sites may be due to slight dealumination, which agrees with the $^{27}Al$ NMR results (see Fig. 2). Next, the loss of intensity at low temperature (~230 °C) can possibly be attributed to the transformation of some of the $Cu^{2+}$ ions to $[Cu(OH)]^+$, according to $H_2$-TPR (see Fig. 3). And $[Cu(OH)]^+$ might adsorb less ammonia compared to $Cu^{2+}$. It could also be related to the small dealumination, which results in less weakly adsorbed ammonia on Al−OH. Overall, it should be noted that even though we observe a small decrease in ammonia storage over Cu/LTA, it maintains the ammonia storage at impressive levels even after hydrothermal aging at 900 °C. This finding can be compared with Cu/SSZ-13 and Cu/BEA, both of which lose a large part of ammonia storage capabilities [17,48].

### 3.2. Reaction results

As depicted in Fig. 10, $NH_3$ oxidation ($4NH_3 + 3O_2 \rightarrow 2N_2 + 6H_2O$) kinetics show some interesting differences for the four degreneed/aged Cu/LTA samples. It can be clearly observed that all the samples are significantly less active for $NH_3$ oxidation, compared with Cu/SSZ-13 treated at similar conditions [53]. For example, less than 11% $NH_3$ conversion at 550 °C can be achieved for the most active Cu/LTA-900. For all samples, $NH_3$ conversions increase gradually with temperature from 250 °C to 550 °C. Notably, when the HTA temperature is increasing, $NH_3$ oxidation ability first decreases, when comparing Cu/LTA-750 and Cu/LTA-800, then slowly increases (Cu/LTA-800 versus Cu/LTA-850). After HTA temperature reaches 900 °C, increase of $NH_3$ conversions can be found more apparent. Due to the need to activate $O_2$, it is generally agreed that only small $CuO_x$ clusters catalyze $NH_3$ and NO oxidation reactions. However, the $H_2$-TPR results in Table 3 show that the population of $CuO_x$ clusters gradually decreases on increasing HTA temperature, which is not identical with $NH_3$ oxidation behavior. However, for $CuO_x$ clusters, one can expect that their activity increases with decreasing cluster size due to increased surface site exposure. Comparing with Cu/LTA-750, Cu/LTA-800 markedly loses $NH_3$ oxidation activity can be explained that after aging at 800 °C, the majority of highly active small $CuO_x$ clusters existing in Cu/LTA-750, contributing most $NH_3$ conversion, are converted to isolated Cu(II) ions, which have low activity for $NH_3$ oxidation. Surprisingly, when HTA temperature is above 800 °C, the ammonia oxidation once again increases despite that the amount of CuOx species are decreasing. According to $H_2$-TPR (see Table 3), the amount of copper in the form ZCuOH is increasing. It is possible that these species in Cu/LTA also show some ammonia oxidation activity, which could explain the increase in ammonia oxidation ability. The same phenomenon is also observed for NO oxidation, as displayed in Fig. S-5.

Fig. 11(a) and (b) presents the standard $NH_3$-SCR ($4NH_3 + 4NO + O_2 \rightarrow 4N_2 + 6H_2O$) light-off curves of NO and the corresponding $NH_3$ conversions for the four Cu/LTA samples aged at different temperatures. It is clear that the NO and $NH_3$ light-off curves almost entirely overlap for all the samples, indicating nearly 100% selectivity in the $NH_3$-SCR reaction. The ability of Cu/LTA to maintain such high selectivity even after hydrothermal aging at 900 °C is outstanding. The same experiments was performed on a corresponding Cu/SSZ-13 sample (Cu/Al = 0.4, Si/Al = 15) and we found a clear deactivation in SCR activity after aging at 850 °C (data not shown). $H_2$-TPR results (shown in Fig. 3) confirm the presence of $CuO_x$ cluster species, which decrease with increasing aging temperature. However, we do not observe any corresponding trend for the high temperature $NO_x$ conversion from the flow reactor experiments, as discussed for the ammonia oxidation experiment. These results indicate that the $CuO_x$ clusters existing in the Cu/LTA samples during the IWI preparation do not affect the high temperature activity. This finding is consistent with the research from Jo et al. [24], which concluded the same. For

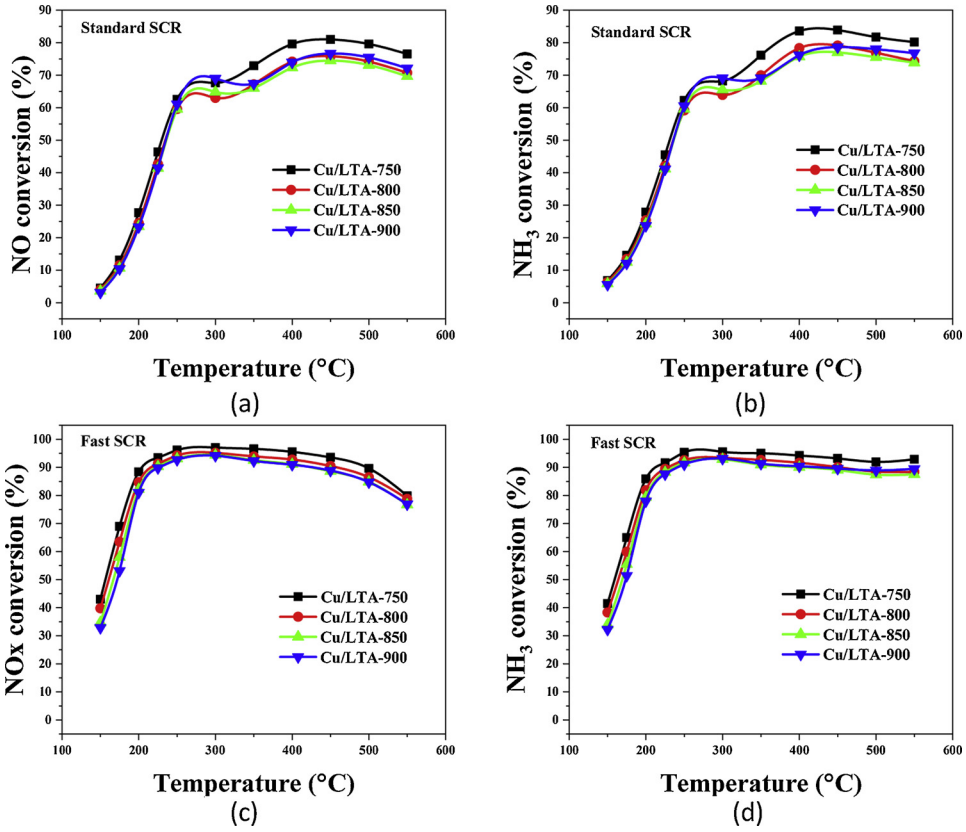


**Fig. 11.** (a), (b) NO and $NH_3$ conversion as a function of temperature during standard $NH_3$-SCR and (c), (d) NO and $NH_3$ conversion as a function of temperature during fast $NH_3$-SCR for Cu/LTA hydrothermally aged at different temperatures. The reactant feed contained 400 ppm NO (or 200 ppm NO and 200 ppm $NO_2$ for fast $NH_3$-SCR), 400 ppm $NH_3$, 10% $O_2$, 5% $H_2O$ balanced with Ar at a GHSV of 22,100 $h^{-1}$.

example, as shown in Fig. 11(a), the $NO_x$ conversion (above 400 °C) for the degreened/aged Cu/LTA catalysts follow the order: 750 > 900 > 800 > 850, while the $NH_3$ oxidation order is 900 > 750 > 850 > 800 (Fig. 10). For many Cu/zeolites an increased ammonia oxidation results in lowering the $NO_x$ selectivity at high temperature, due to competitive ammonia oxidation. However, this is not the case for the Cu/LTA sample, where for example Cu/LTA-900 has the highest ammonia oxidation, but still the second highest $NO_x$ conversion at high temperature. The reason for this could be the low activity for ammonia oxidation on Cu/LTA samples (less than 11% at 550 °C), which results in that ammonia is still available also at the higher temperatures (see Fig. 11b). Thus, the SCR reaction is not limited by ammonia availability.

Second key finding was the slightly improved activity at the temperature region of 250– 350 °C which can be observed upon aging, especially for the samples of Cu/LTA-800, 850 and 900. This might be explained by the transformation of $CuO_x$ clusters to Cu(II) species, which results in more active sites, in line with the $H_2$-TPR results (see Fig. 3). However, the exception is Cu/LTA-750, that has similar activity as Cu/LTA-900 in this temperature region. This suggests that the content of Cu(II) species is not the only reason for activity change at the region of 250–350 °C. The different activities towards SCR reactions, e.g., $Cu^{2+}$ is possibly more active than $[Cu(OH)]^+$, could also play an important role.

Additionally, Fig. 11(c) and (d) compare light-off curves in fast $NH_3$-SCR ($2NH_3 + NO + NO_2 \rightarrow 2N_2 + 3H_2O$) for the four samples. To our knowledge, this is the first time that the effect of aging for Cu/LTA is showed for fast $NH_3$-SCR reaction. The four Cu/LTA samples have an outstanding $NO_x$ reduction efficiency in a broad temperature window of 200–500 °C and in addition remarkably stable. The high conversion and high temperature stability make Cu/LTA one of the best candidates for fast $NH_3$-SCR reaction compared with Cu/zeolites or Fe/zeolites previously reported in literature [54–56]. It should be highlighted that the direct comparison between standard SCR and fast SCR demonstrates that non-selective $NH_3$ oxidation is promoted to some extent by the presence of $NO_2$ at high temperature. For example, at 550 °C, $NH_3$ conversions via non-selective $NH_3$ oxidation in fast $NH_3$-SCR are higher than conversions in the standard $NH_3$-SCR. This can be described by a reaction between $NO_2$ and ammonia to produce NO, which was proposed by Watling et al. [57] in a kinetic model for Cu/zeolites and also experimentally verified in one of our earlier studies [58].

The effect of hydrothermal aging on Cu/LTA and its influence on $N_2O$ formation are displayed in Fig. 12(a) for standard $NH_3$-SCR and Fig. 12(b) for fast $NH_3$-SCR. As for Cu/SSZ-13, a low temperature peak at ~250 °C is observed. This peak can most likely be attributed to the decomposition of $NH_4NO_3$/ammonium nitrate precursor species [52], for both SCR reactions [11]. At elevated temperatures (≥ 350 °C), $N_2O$ formation increases again, which is also observed for Cu/SSZ-13 [52]. Note that, during ammonia oxidation experiment, the maximum $N_2O$ amount is 1–2 ppm, while it is significantly larger during standard SCR (~18 ppm) and fast SCR (~34 ppm) for Cu/LTA-750. Thus, these results show that most of the $N_2O$ comes from the reaction between $NO_x$ (i.e., NO and $NO_2$) and $NH_3$ directly and not from un-selective ammonia oxidation. The results reveal that the fast SCR results in larger $N_2O$ amount than standard SCR, which is consistent with other copper zeolites [58]. Moreover, the amount of $N_2O$ is increasing with increasing hydrothermal aging, especially at high temperatures.

Next, Fig. 13 depicts TPD results of different gas outlets (NO, $NO_2$, $N_2O$ and $NH_3$) following the fast SCR experiment. To facilitate comparison, the gases for each aging temperature, are presented in Fig. S-6. For all four Cu/LTA samples, extremely weak NO desorption peaks (< 15 ppm) are found at ~240 and 510 °C, as shown in Fig. 13(a). This could be assigned to weakly adsorbed NO and possibly also to the decomposition of ammonium nitrate species.

Fig. 13(b) and (c) present the desorption curves for $NO_2$ and $N_2O$, both primarily centered at ~240 and 290 °C, respectively. It is worth noting that the amount of $NO_2$ and $N_2O$ produced affected in the opposite direction with the increase of aging temperature. $NO_2$ outlet

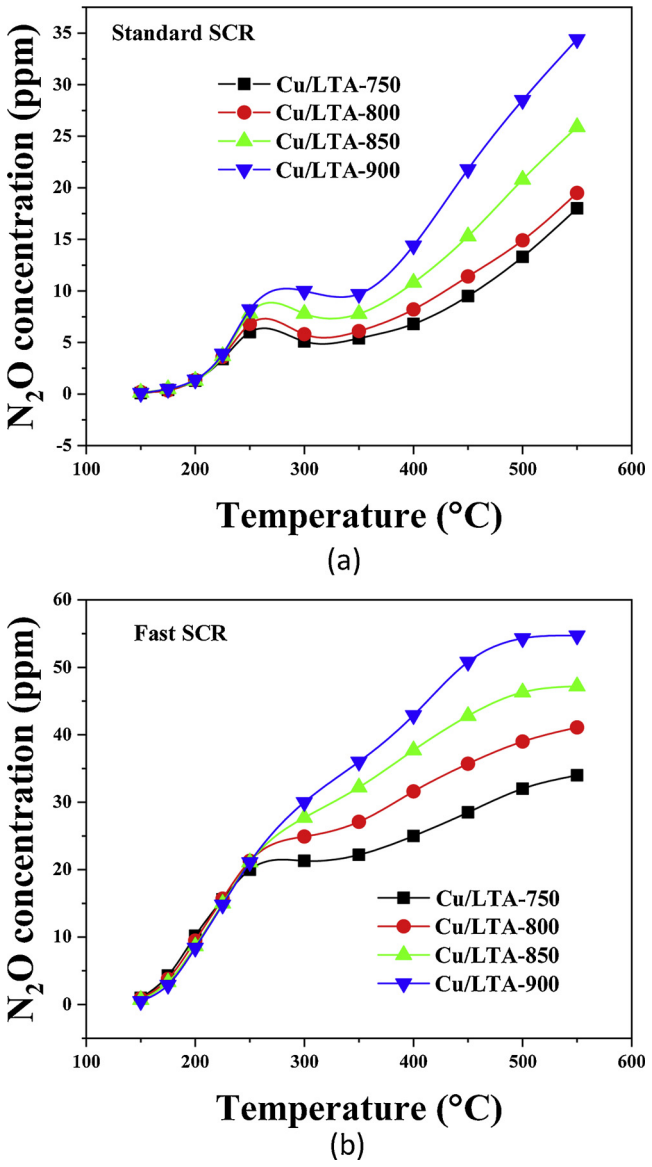


**Fig. 12.** $N_2O$ outlet concentrations measured during (a) standard $NH_3$-SCR and (b) fast $NH_3$-SCR. The reactant feed contained 400 ppm NO (or 200 ppm NO and 200 ppm $NO_2$ for fast $NH_3$-SCR), 400 ppm $NH_3$, 10% $O_2$, 5% $H_2O$ balanced with Ar at a GHSV of 22,100 $h^{-1}$.

concentration increases with elevating aging temperature, whereas $N_2O$ decreases gradually. The typical decomposition path of $NH_4NO_3$ is as follows [59]:

$$NH_4NO_3 \rightarrow N_2O + 2H_2O \quad (4)$$

which produces $N_2O$, as shown in Fig. 13(b). Also, according to the previous study by Peden et al. [60], another pathway for $NH_4NO_3$ decomposition is existing, which produces $NO_2$ as below:

$$NH_4NO_3 \rightarrow NH_4^+ + O^- + NO_2 \quad (5)$$

Based on the above discussion, two key points can be concluded: (i) a shift in reaction path for $NH_4NO_3$ decomposition can be found with increasing HTA temperature, and this is generally from Reaction (4) to Reaction (5). (ii) decomposition according to Reaction (5) is more important at lower temperature (230–240 °C), whereas at higher temperature (280–290 °C), Reaction (4) is dominant. Notably, a weak $NO_2$ desorption state is observed at ~430 °C for Cu/LTA-750 and Cu/LTA-800. As HTA temperature increases, the peak shifts to lower temperature (~350 °C) for Cu/LTA-850 and Cu/LTA-900.

Moreover, a large $NH_3$ desorption is observed at ~220 °C, which can be attributed to the ammonia adsorbed on the Cu(II) sites and also a small desorption is found from Brønsted acid sites at higher temperature (~300 °C) as displayed in Fig. 13(d). It should be noted that some of the ammonia desorbed will also originate from decomposition of ammonium nitrates, according to Reaction (5). And also a part of the ammonia can react with the released $NO_2$, which is known as slow $NO_2$ SCR reaction. The amount of $NH_3$ decreases with increasing aging temperature which is consistent with $NH_3$-TPD displayed in Fig. 9, and it is consistent with the small dealumination that is observed (Fig. 2). The big difference when comparing with $NH_3$-TPD is that the intensity of $NH_3$ desorption peak from Brønsted acid sites is much lower and this can be explained by (i) some of the Brønsted acid sites are blocked by $NH_4NO_3$, which have a lower decomposition temperature and (ii) some of the stored ammonia might react with released $NO_2$ in $NO_2$ SCR reaction.

## 4. Conclusions

To summarize, Cu/LTA catalysts were synthesized using the incipient wetness impregnation (IWI) method, and degreened/hydrothermally aged at 750, 800, 850 and 900 °C to investigate the reason for their outstanding hydrothermal stability. The catalysts were used to study standard SCR, fast SCR and $NH_3$/NO oxidation reactions. Multiple characterization methods, including BET, XRD, NMR, $H_2$-TPR, DRIFTS, $NH_3$-TPD were used to characterize the samples.

After harsh aging up to 900 °C, the catalytic activity and zeolite structure of the samples were well maintained. This result suggests that the Cu/LTA synthesized in this study can be used as a model catalyst for in-depth study of the unique stability. One key finding from this study is the extraordinary thermal stability of $[Cu(OH)]^+$, which was not converted to $Cu^{2+}$ and $CuO_x$ clusters upon aging, like Cu-SSZ/13. On the contrary, parts of $Cu^{2+}$ and $CuO_x$ clusters gradually transformed into $[Cu(OH)]^+$ with elevating the aging temperature. As we know, the formation of $CuO_x$ clusters in Cu/SSZ-13 is the primary reason for the subsequent decline in catalyst selectivity and structural collapse. We suggest that this difference in the behavior of copper species upon hydrothermal aging is one of the reasons for the extraordinary hydrothermal stability of Cu/LTA samples. Further, we found that Cu/LTA is also a promising fast-SCR catalyst, with a broad temperature window of 200–500 °C, capable of even undertaking serious hydrothermal aging (e.g., 900 °C). Moreover, we found that the hydrothermal aging shifted the pathway of $NH_4NO_3$ decomposition.

## Acknowledgements

This study was performed at the Division of Chemical Engineering and the Competence Centre for Catalysis, Chalmers University of Technology in collaboration with Cummins Inc. The financial support of Cummins Inc. and the Swedish Research Council (642-2014-5733) are gratefully acknowledged. The Chalmers Materials Analysis Laboratory is acknowledged for SEM access. We would also like to acknowledge Prof. Suk Bong and Dr Donghui Jo at Pohang University of Science and Technology (POSTECH) for helpful advice regarding LTA synthesis. The Knut and Alice Wallenberg Foundation is acknowledged for access and support to the “NMR for Life” facility at Umeå University and thanks for the help of Dr Tobias Sparrman.

## Appendix A. Supplementary data

Supplementary material related to this article can be found, in the online version, at doi:https://doi.org/10.1016/j.apcatb.2019.01.039.

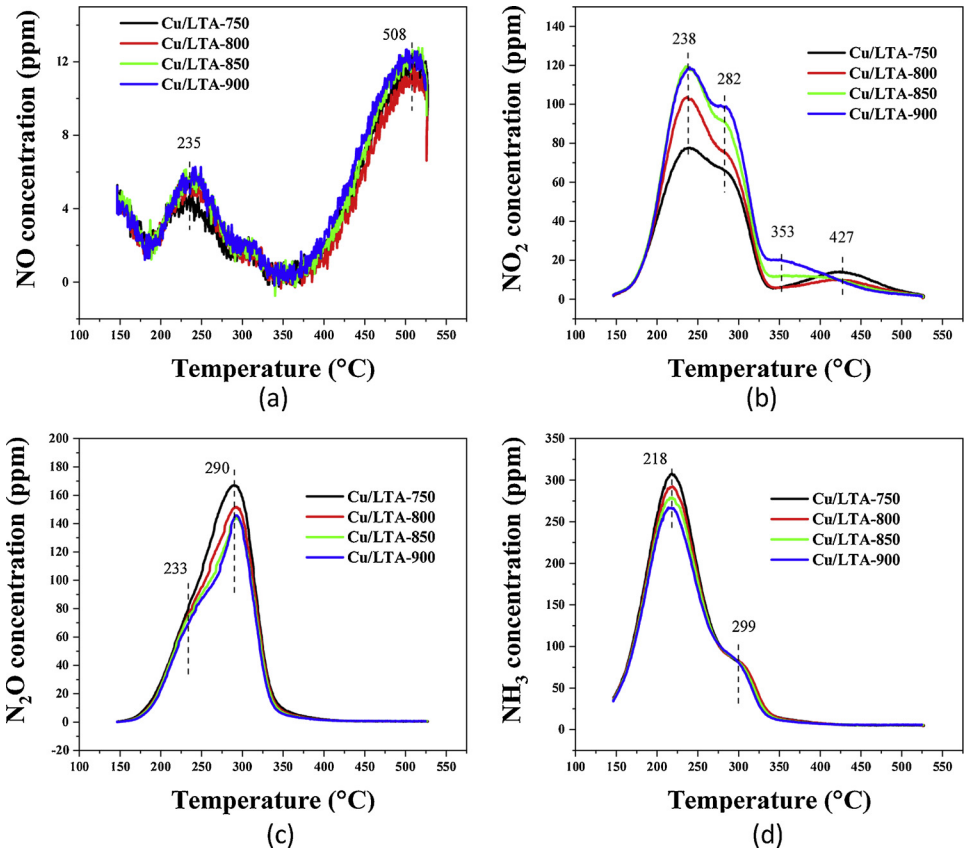


**Fig. 13.** Temperature Programmed Desorption (TPD) after Fast SCR for Cu/LTA hydrothermally aged at different temperatures with (a) NO, (b) $NO_2$, (c) $N_2O$ and (d) $NH_3$ outlet concentrations.

## References


[1] J. Song, Y.L. Wang, E.D. Walter, N.M. Washton, D.H. Mei, L. Kovarik, M.H. Engelhard, S. Prodinger, Y. Wang, C.H.F. Peden, F. Gao, Toward rational design of Cu/SSZ-13 selective catalytic reduction catalysts: implications from atomic-level understanding of hydrothermal stability, ACS Catal. 7 (2017) 8214–8227.

[2] N. Takahashi, H. Shinjoh, T. Iijima, T. Suzuki, K. Yamazaki, K. Yokota, H. Suzuki, N. Miyoshi, S.-i. Matsumoto, T. Tanizawa, The new concept 3-way catalyst for automotive lean-burn engine: $NO_x$ storage and reduction catalyst, Catal. Today 27 (1996) 63–69.

[3] D.L. Mowery, M.S. Graboski, T.R. Ohno, R.L. McCormick, Deactivation of PdO–$Al_2O_3$ oxidation catalyst in lean-burn natural gas engine exhaust: aged catalyst characterization and studies of poisoning by $H_2O$ and $SO_2$, Appl. Catal. B: Environ. 21 (1999) 157–169.

[4] J.Y. Jeon, H.Y. Kim, S.I. Woo, Selective catalytic reduction of $NO_x$ in lean-burn engine exhaust over a Pt/V/MCM-41 catalyst, Appl. Catal. B: Environ. 44 (2003) 311–323.

[5] L. Landong, C. Jixin, Z. Shujuan, Z. Fuxiang, G. Naijia, W. Tianyou, L. Shuliang, Selective catalytic reduction of nitrogen oxides from exhaust of lean burn engine over in-situ synthesized Cu−ZSM-5/cordierite, Environ. Sci. Technol. 39 (2005) 2841–2847.

[6] A. Wang, Y. Wang, E.D. Walter, R.K. Kukkadapu, Y. Guo, G. Lu, R.S. Weber, Y. Wang, C.H. Peden, F. Gao, Catalytic $N_2O$ decomposition and reduction by $NH_3$ over Fe/Beta and Fe/SSZ-13 catalysts, J. Catal. 358 (2018) 199–210.

[7] L. Kovarik, N.M. Washton, R. Kukkadapu, A. Devaraj, A.Y. Wang, Y.L. Wang, J. Szanyi, C.H.F. Peden, F. Gao, Transformation of active sites in Fe/SSZ-13 SCR catalysts during hydrothermal aging: a spectroscopic, microscopic, and kinetics study, ACS Catal. 7 (2017) 2458–2470.

[8] O. Mihai, C.R. Widyastuti, S. Andonova, K. Kamasamudram, J. Li, S.Y. Joshi, N.W. Currier, A. Yezerets, L. Olsson, The effect of Cu-loading on different reactions involved in $NH_3$-SCR over Cu-BEA catalysts, J. Catal. 311 (2014) 170–181.

[9] C. Paolucci, I. Khurana, A.A. Parekh, S.C. Li, A.J. Shih, H. Li, J.R. Di Iorio, J.D. Albarracin-Caballero, A. Yezerets, J.T. Miller, W.N. Delgass, F.H. Ribeiro, W.F. Schneider, R. Gounder, Dynamic multinuclear sites formed by mobilized copper ions in NOx selective catalytic reduction, Science 357 (2017) 898–903.

[10] A. Marberger, A.W. Petrov, P. Steiger, M. Elsener, O. Krocher, M. Nachtegaal, D. Ferri, Time-resolved copper speciation during selective catalytic reduction of NO on Cu-SSZ-13, Nat. Catal. 1 (2018) 221–227.

[11] A. Wang, Y. Wang, E.D. Walter, N.M. Washton, Y. Guo, G. Lu, C.H. Peden, F. Gao, $NH_3$-SCR on Cu, Fe and Cu + Fe exchanged beta and SSZ-13 catalysts: hydrothermal aging and propylene poisoning effects, Catal. Today 320 (2019) 91–99.

[12] J. Wang, T. Yu, X. Wang, G. Qi, J. Xue, M. Shen, W. Li, The influence of silicon on the catalytic properties of Cu/SAPO-34 for $NO_x$ reduction by ammonia-SCR, Appl. Catal. B: Environ. 127 (2012) 137–147.

[13] D. Wang, L. Zhang, J. Li, K. Kamasamudram, W.S. Epling, $NH_3$-SCR over Cu/SAPO-34–zeolite acidity and Cu structure changes as a function of Cu loading, Catal. Today 231 (2014) 64–74.

[14] U. De-La-Torre, B. Pereda-Ayo, M. Moliner, J.R. González-Velasco, A. Corma, Cu-zeolite catalysts for $NO_x$ removal by selective catalytic reduction with $NH_3$ and coupled to NO storage/reduction monolith in diesel engine exhaust after treatment systems, Appl. Catal. B: Environ. 187 (2016) 419–427.

[15] A.M. Beale, F. Gao, I. Lezcano-Gonzalez, C.H. Peden, J. Szanyi, Recent advances in automotive catalysis for $NO_x$ emission control by small-pore microporous materials, Chem. Soc. Rev. 44 (2015) 7371–7405.

[16] J.H. Kwak, D. Tran, S.D. Burton, J. Szanyi, J.H. Lee, C.H. Peden, Effects of hydrothermal aging on $NH_3$-SCR reaction over Cu/zeolites, J. Catal. 287 (2012) 203–209.

[17] K. Leistner, A. Kumar, K. Kamasamudram, L. Olsson, Mechanistic study of hydrothermally aged Cu/SSZ-13 catalysts for ammonia-SCR, Catal. Today 307 (2018) 55–64.

[18] G.E.D.W. Breckw, M. Miltont, B. Reeda, N.D.T.L. Thomas, Crystalline zeolites. I. The properties of a new synthetic zeolite, type A, J. Am. Chem. Soc. 78 (1956) 5963.

[19] E. Jaramillo, M. Chandross, Adsorption of small molecules in LTA zeolites. 1. $NH_3$, $CO_2$, and $H_2O$ in zeolite 4A, J. Phys. Chem. B 108 (2004) 20155–20159.

[20] M. Palomino, A. Corma, F. Rey, S. Valencia, New insights on CO2-methane separation using LTA zeolites with different Si/Al ratios and a first comparison with MOFs, Langmuir 26 (2010) 1910–1917.

[21] T. Montanari, I. Salla, G. Busca, Adsorption of CO on LTA zeolite adsorbents: an IR investigation, Microporous Mesoporous Mater. 109 (2008) 216–222.

[22] A. Corma, F. Rey, J. Rius, M.J. Sabater, S. Valencia, Supramolecular self-assembled molecules as organic directing agent for synthesis of zeolites, Nature 431 (2004) 287–290.

[23] B.W. Boal, J.E. Schmidt, M.A. Deimund, M.W. Deem, L.M. Henling, S.K. Brand, S.I. Zones, M.E. Davis, Facile synthesis and catalysis of pure-silica and heteroatom LTA, Chem. Mater. 27 (2015) 7774–7779.

[24] D. Jo, T. Ryu, G.T. Park, P.S. Kim, C.H. Kim, I.S. Nam, S.B. Hong, Synthesis of high-silica LTA and UFI zeolites and NH3-SCR performance of their copper-exchanged form, ACS Catal. 6 (2016) 2443–2447.

[25] T. Ryu, N.H. Ahn, S. Seo, J. Cho, H. Kim, D. Jo, G.T. Park, P.S. Kim, C.H. Kim, E.L. Bruce, P.A. Wright, I.S. Nam, S.B. Hong, Fully copper-exchanged high-silica LTA zeolites as unrivaled hydrothermally stable NH3-SCR catalysts, Angew. Chem. Int. Ed. Engl. 56 (2017) 3256–3260.

[26] S. Shwan, M. Skoglundh, L.F. Lundegaard, R.R. Tiruvalam, T.V. Janssens, A. Carlsson, P.N. Vennestrøm, Solid-state ion-exchange of copper into zeolites facilitated by ammonia at low temperature, ACS Catal. 5 (2014) 16–19.
[27] J. Woo, K. Leistner, D. Bernin, H. Ahari, M. Shost, M. Zammit, L. Olsson, Effect of various structure directing agents (SDAs) on low-temperature deactivation of Cu/SAPO-34 during $NH_3$-SCR reaction, Catal. Sci. Technol. 8 (2018) 3090–3106.
[28] A. Shishkin, P.-A. Carlsson, H. Härelind, M. Skoglundh, Effect of preparation procedure on the catalytic properties of Fe-ZSM-5 as SCR catalyst, Top. Catal. 56 (2013) 567–575.
[29] X. Auvray, L. Olsson, Stability and activity of Pd-, Pt-and Pd–Pt catalysts supported on alumina for NO oxidation, Appl. Catal. B: Environ. 168 (2015) 342–352.
[30] S. Prodinger, M.A. Derewinski, Y.L. Wang, N.M. Washton, E.D. Walter, J. Szanyi, F. Gao, Y. Wang, C.H.F. Peden, Sub-micron Cu/SSZ-13: synthesis and application as selective catalytic reduction (SCR) catalysts, Appl. Catal. B-Environ. 201 (2017) 461–469.
[31] F. Gao, E.D. Walter, E.M. Karp, J.Y. Luo, R.G. Tonkyn, J.H. Kwak, J. Szanyi, C.H.F. Peden, Structure-activity relationships in $NH_3$-SCR over Cu-SSZ-13 as probed by reaction kinetics and EPR studies, J. Catal. 300 (2013) 20–29.
[32] L. Wang, W. Li, G. Qi, D. Weng, Location and nature of Cu species in Cu/SAPO-34 for selective catalytic reduction of NO with $NH_3$, J. Catal. 289 (2012) 21–29.
[33] B. Pereda-Ayo, U. De La Torre, M.J. Illán-Gómez, A. Bueno-López, J.R. González-Velasco, Role of the different copper species on the activity of Cu/zeolite catalysts for SCR of $NO_x$ with $NH_3$, Appl. Catal. B: Environ. 147 (2014) 420–428.
[34] S.T. Korhonen, D.W. Fickel, R.F. Lobo, B.M. Weckhuysen, A.M. Beale, Isolated $Cu^{2+}$ ions: active sites for selective catalytic reduction of NO, Chem. Commun. 47 (2011) 800–802.
[35] U. Deka, Al. Juhin, E.A. Eilertsen, H. Emerich, M.A. Green, S.T. Korhonen, B.M. Weckhuysen, A.M. Beale, Confirmation of isolated $Cu^{2+}$ ions in SSZ-13 zeolite as active sites in $NH_3$-selective catalytic reduction, J. Phys. Chem. C 116 (2012) 4809–4818.
[36] R. Bulánek, B. Wichterlová, Z. Sobalık, J. Tichý, Reducibility and oxidation activity of Cu ions in zeolites: effect of Cu ion coordination and zeolite framework composition, Appl. Catal. B: Environ. 31 (2001) 13–25.
[37] J.H. Kwak, H. Zhu, J.H. Lee, C.H. Peden, J. Szanyi, Two different cationic positions in Cu-SSZ-13? Chem. Commun. 48 (2012) 4758–4760.
[38] Y. Jangjou, Q. Do, Y.T. Gu, L.G. Lim, H. Sun, D. Wang, A. Kumar, J.H. Li, L.C. Grabow, W.S. Epling, Nature of Cu active centers in Cu-SSZ-13 and their responses to SO2 exposure, ACS Catal. 8 (2018) 1325–1337.
[39] S.S.R. Putluru, A. Riisager, R. Fehrmann, Alkali resistant Cu/zeolite de$NO_x$ catalysts for flue gas cleaning in biomass fired applications, Appl. Catal. B: Environ. 101 (2011) 183–188.
[40] F. Gao, N.M. Washton, Y.L. Wang, M. Kollar, J. Szanyi, C.H.F. Peden, Effects of Si/Al ratio on Cu/SSZ-13 $NH_3$-SCR catalysts: implications for the active Cu species and the roles of Bronsted acidity, J. Catal. 331 (2015) 25–38.
[41] W. Su, Z. Li, Y. Peng, J. Li, Correlation of the changes in the framework and active Cu sites for typical Cu/CHA zeolites (SSZ-13 and SAPO-34) during hydrothermal aging, Phys. Chem. Chem. Phys. 17 (2015) 29142–29149.
[42] D. Wang, F. Gao, C.H.F. Peden, J.H. Li, K. Kamasamudram, W.S. Epling, Selective catalytic reduction of $NO_x$ with $NH_3$ over a Cu-SSZ-13 catalyst prepared by a solid-state ion-exchange method, ChemCatChem 6 (2014) 1579–1583.
[43] J.Y. Luo, F. Gao, K. Kamasamudram, N. Currier, C.H.F. Peden, A. Yezerets, New insights into Cu/SSZ-13 SCR catalyst acidity. Part I: nature of acidic sites probed by $NH_3$ titration, J. Catal. 348 (2017) 291–299.
[44] Y. Peng, C. Wang, K. Li, S. Liu, X. Li, J. Chen, J. Li, Selective catalytic reduction of $NO_x$ with ammonia over novel Cu ion-exchanged SAPO-47 zeolites in a wide temperature range, ChemCatChem 10 (2018) 2481–2487.
[45] S. Bordiga, L. Regli, D. Cocina, C. Lamberti, M. Bjørgen, K.P. Lillerud, Assessing the acidity of high silica chabazite H− SSZ-13 by FTIR using CO as molecular probe: comparison with H− SAPO-34, J. Phys. Chem. B 109 (2005) 2779–2784.
[46] W. Su, H. Chang, Y. Peng, C. Zhang, J. Li, Reaction pathway investigation on the selective catalytic reduction of NO with $NH_3$ over Cu/SSZ-13 at low temperatures, Environ. Sci. Technol. 49 (2014) 467–473.
[47] E. Borfecchia, K. Lomachenko, F. Giordanino, H. Falsig, P. Beato, A. Soldatov, S. Bordiga, C. Lamberti, Revisiting the nature of Cu sites in the activated Cu-SSZ-13 catalyst for SCR reaction, Chem. Sci. 6 (2015) 548–563.
[48] N. Wilken, K. Wijayanti, K. Kamasamudram, N.W. Currier, R. Vedaiyan, A. Yezerets, L. Olsson, Mechanistic investigation of hydrothermal aging of Cu-beta for ammonia SCR, Appl. Catal. B 111 (2012) 58.
[49] S.A. Bates, W.N. Delgass, F.H. Ribeiro, J.T. Miller, R. Gounder, Methods for $NH_3$ titration of Brønsted acid sites in Cu-zeolites that catalyze the selective catalytic reduction of $NO_x$ with $NH_3$, J. Catal. 312 (2014) 26–36.
[50] K. Leistner, K. Xie, A. Kumar, K. Kamasamudram, L. Olsson, Ammonia desorption peaks can be assigned to different copper sites in Cu/SSZ-13, Catal. Lett. 147 (2017) 1882–1890.
[51] C. Niu, X. Shi, F. Liu, K. Liu, L. Xie, Y. You, H. He, High hydrothermal stability of Cu–SAPO-34 catalysts for the $NH_3$-SCR of $NO_x$, Chem. Eng. J. 294 (2016) 254–263.
[52] L. Olsson, K. Wijayanti, K. Leistner, A. Kumar, S. Joshi, K. Kamasamudram, N.W. Currier, A. Yezerets, A multi-site kinetic model for $NH_3$-SCR over Cu/SSZ-13, Appl. Catal. B: Environ. 174–175 (2015) 212.
[53] D. Wang, Y. Jangjou, Y. Liu, M.K. Sharma, J. Luo, J. Li, K. Kamasamudram, W.S. Epling, A comparison of hydrothermal aging effects on $NH_3$-SCR of $NO_x$ over Cu-SSZ-13 and Cu-SAPO-34 catalysts, Appl. Catal. B: Environ. 165 (2015) 438–445.
[54] M. Iwasaki, H. Shinjoh, A comparative study of “standard”, “fast” and “$NO_2$” SCR reactions over Fe/zeolite catalyst, Appl. Catal. A: Gen. 390 (2010) 71–77.
[55] R.P. Vélez, I. Ellmers, H. Huang, U. Bentrup, V. Schünemann, W. Grünert, A. Brückner, Identifying active sites for fast $NH_3$-SCR of NO/$NO_2$ mixtures over Fe-ZSM-5 by operando EPR and UV–vis spectroscopy, J. Catal. 316 (2014) 103–111.
[56] L. Xie, F. Liu, K. Liu, X. Shi, H. He, Inhibitory effect of $NO_2$ on the selective catalytic reduction of NOx with $NH_3$ over one-pot-synthesized Cu–SSZ-13 catalyst, Catal. Sci. Technol. 4 (2014) 1104–1110.
[57] T.C. Watling, M.R. Ravenscroft, G. Avery, Development, validation and application of a model for an SCR catalyst coated diesel particulate filter, Catal. Today 188 (2012) 32–41.
[58] O. Mihai, C.R. Widyastuti, A. Kumar, J. Li, S.Y. Joshi, K. Kamasamudram, N.W. Currier, A. Yezerets, L. Olsson, The effect of $NO_2/NO_x$ feed ratio on the $NH_3$-SCR system over Cu-zeolites with varying loading, Catal. Lett. 144 (1) (2014) 70.
[59] A. Grossale, I. Nova, E. Tronconi, Ammonia blocking of the “Fast SCR” reactivity over a commercial Fe-zeolite catalyst for diesel exhaust after treatment, J. Catal. 265 (2009) 141–147.
[60] F. Gao, Y.L. Wang, M. Kollar, N.M. Washton, J. Szanyi, C.H.F. Peden, A comparative kinetics study between Cu/SSZ-13 and Fe/SSZ-13 SCR catalysts, Catal. Today 258 (2015) 347–358.